Brief communication - –Vent opening at Campi Flegrei: clues from dyke propagation patterns

Jacopo Selva[1], Nello Mangone[1]

[1] Dipartimento di Scienze della Terra, dell'Ambiente e delle Risorse (DiSTAR), University of Naples Federico II, Naples Italy

Correspondence to: Jacopo Selva (jacopo.selva@unina.it)

Abstract. Forecasting future vent opening position is fundamental for managing volcanic hazards, and is usually based on the spatial density of past vents or other crust weakness indicators. Here, a novel empirical approach inspired by dyke propagation models is applied to the Campi Flegrei caldera. Results show that dyke azimuthal direction and propagation length are statistically independent, that azimuth correlates with topographic peaks within 67 km from the caldera centercentre, and that propagation length exhibits two main peaks at 2 and 4 km. Based on these results, leading to awe develop two new vent opening probability mapmaps with maxima well correlating with caldera's structure and recent major seismicity and deformations.

1 Introduction

The Campi Flegrei caldera volcanic activity dates back to the upper Pleistocene, with the oldestearliest volcanic activity observed in outcrops estimated at aroundapproximately 80 kyr (Pappalardo et al. 1999; Scarpati et al. 2013). Recent studies identified widespread tephra layers originated from Campi Flegrei,000 years ago extending its activity to nearly 200 kyr (D'Antonioe.g., Monaco et al., 2022; Fernandez et al., 20072024; OrsiSparice et al. 2009, 2024). The first caldera collapse occurred approximately 39,000 years ago with the Campanian Ignimbrite (CI) eruption (Giaccio et al. The period following the CI is characterised by eruptions confined within the newly formed caldera, both continental and marine2017). A second major eruption occurred around 14,000 years ago, the Neapolitan Yellow Tuff (NYT), which likely causedpossibly causing a second collapse that shaped the current caldera structure (Sbrana et al., 2021). After the NYT eruption,after which volcanic activity resumed within the inner caldera (Orsi et al. 2004).

The post-NYT eruptive history is divided into three main epochs (Di Vito et al. 1999, Bevilacqua et al. 2016, Fig. 1). The first epoch comprises a total ofat least 33 eruptions, spaningspanning from 1514,000 to 10,600 years ago. The eruptive vents align with the newly formed caldera boundaries, with the most energetic eruption being that of the "Pomici Principali" around 12,300000 years ago (Bevilacqua et al. 2016). The second epoch follows a relatively brief quiescent period and includes nine eruptions dated between 9,600 and 9,200100 years ago, primarily concentrated in the northeastern sector of the caldera. The third epoch encompasses a total of 2826 eruptions from approximately 5,500 to 3,800 years ago; this epoch is. Its activity was

predominantly focused in the northeastern part of the caldera (Agnano area) ~~and,~~ secondarily in the northwestern sector (Averno area), and concluded with peripheral distal eruptions (Nisida, Capo Miseno, and Fossa Lupara (Natale et al., 2025). The most energetic eruption during this period was that of Agnano-Monte Spina around 4,~~550~~500 years ago (Bevilacqua et al. 2016). The long period of quiescence following the third epoch lasted until 1538 AD, when the Monte Nuovo eruption took place in the northwestern sector of the caldera (Di Vito et al., ~~1999~~2016). The caldera has not experienced any eruption since. After NYT, the caldera experienced significant resurgence, accompanied by seismicity, degassing, and slow ground deformation often referred to as bradyseism (Isaia et al., 2019; Natale et al., 2022). The latter is ~~concentrated~~centred mainly in the Pozzuoli area, which is approximately at the ~~geometrical center~~centre of the caldera~~, in the Pozzuoli area~~ (Fig. 1), and major movements were tracked at least from the 4th century AD thanks to the ruins of a Roman temple in the port of this city, known as the Serapeum (Di Vito et al. 2016; Natale et al. 2023). The largest known bradyseismic events are the ones related to the last Campi Flegrei eruption (the 1538 Monte Nuovo eruption, Di Vito et al., ~~1999~~2016). In the last century, three main bradyseismic crises occurred in 1950-52, 1970-72, and ~~1984-86~~1982-84, characterised by episodes of uplift of more than 1 m interrupting a slow long-lasting subsidence (Del Gaudio et al 2010). Approximately in 2005, a slow uplift started, accelerating over time, which ~~now~~ fully recovered the subsidence in 2021, ~~exceeding~~and now exceeds the uplift peaks observed in the last century (~~Chiodini et al. 2021,~~ Bevilacqua et al. 2024~~, Giudicepietro et al. 2025~~). This event is still ongoing.

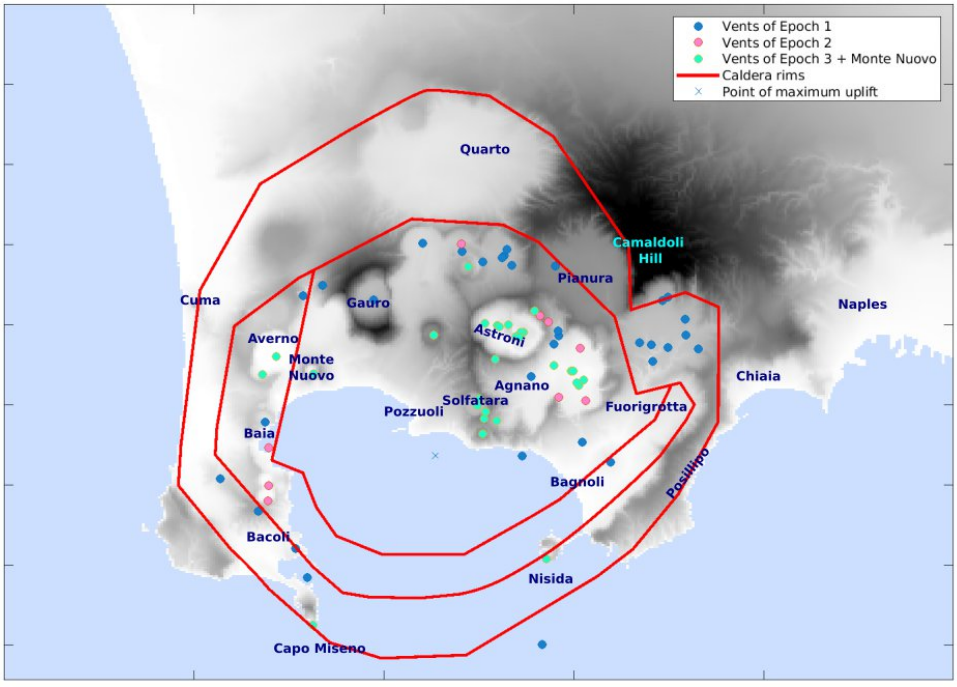

¶

Figure 1: Toponymic the Campi Flegrei caldera, along with the vent positions of post-NYT eruptions (from Bevilacqua et al. 2016) and the caldera rims (Natale et al. 2024, 2025). For simplicity, Monte Nuovo is included in Epoch 3.¶

¶

¶

Forecasting vent opening is crucial for any volcanic hazard quantification, especially in calderas. Different approaches were adopted at Campi Flegrei through time. Alberico et al. (2002) developed a method identifying crustal weaknesses using geophysical, geological, and geochemical parameters. Their probability map ~~indicated~~indicates the highest likelihood of vent openings in the central caldera near Pozzuoli (Fig. 1). Selva et al. (2012) utilized a Bayesian approach fed by fewer parameters, focusing on tectonic structures recognized at that time, to track crust weakness, and past vents, shifting the area at higher probability toward the northeastern and northwestern sectors, where post-NYT activity concentrated. Bevilacqua et al. (2015) adopted a method based on Gaussian kernel and accounting for the uncertainty on past vent positions, confirming the northeastern sector (near Agnano and Astroni, Fig. 1) as the most likely area for future eruptions. Both Selva et al. (2012) and Bevilacqua et al. (2015) included also a formal quantification of the epistemic uncertainty in their models, accounting for model uncertainty. More recently, based on past observations and removing multiple eruptions from clustered vents, Charlton et al. (~~2018~~2020) noted that vent opening occurred substantially randomly within a ring area surrounding the caldera ~~center~~centre, corresponding to the ~~NYT ring~~caldera rim (Fig. 1), producing a new qualitative indication about potential future vent opening.

Rivalta et al. (2019) studied the physical propagation of magma ~~dikes~~dykes by modelling the trajectory of potential ~~dikes~~ dykes due to the subsurface stress field and the dike's initial position. Their model accounts for various stresses affecting magma ascent. For calderas, it suggests that eruptive vents are concentrated at specific distances from the centre, influenced by the stress induced by the caldera depression, defining a higher propensity to eruption closer to caldera rims, as noted by Charlton et al. (2020). Considering the caldera depression size, Rivalta et al. (2019) forecasted for Campi Flegrei a potential peak for vent opening at a semiannular belt located between 2.3 and 4.2 km from the caldera ~~center~~centre. Rivalta et al. (2019) ~~analyzed also~~analysed the effect of caldera unloading, as well as those of topographic peaks, which may break the caldera symmetry. They ~~analyzed~~analysed the case of the Campi Flegrei caldera, explaining the concentration of volcanic activity in the northeastern sector due to the peak of the Camaldoli ~~hill~~Hill (Fig. 1), which creates a stress field ~~favouring~~that may favour magma trajectories in the ~~northeast~~north-east direction.

The main features of Rivalta et al. (2019) model are i) that the geometry of the caldera (unloading effect) significantly influences ~~dike~~ dykes propagation outward, promoting eruptions away from the geometric centre ~~a a given distance~~of the caldera, and ii) topographic asymmetries create localised stress variations in the subsurface, affecting eruption frequency across different angular sectors. While a sufficiently detailed knowledge of the sub-surface stress state is difficult to reach, it is possible to verify if these two main features left ~~track~~a trace on the available record of past vent positions, and to use this empirical signature to define new vent opening probability maps.

2 ~~Empirical distribution of direction and length of past dykes~~Method

~~The~~Rivalta et al. (2019) found that the path of the dykes feeding ~~past~~ eruptions is mainly controlled by the geometry of the caldera, which determines the distance from the centre of the caldera, and by the topographical peaks surrounding the caldera, which establishes preferential directions for propagation. ~~Assuming~~To this end, Rivalta et al. (2019) assumed that the origin at depth of the magma is located at the centre of the caldera, 3 km below the location of the maximum observed uplift (Amoruso et al. ~~2012~~2014, Rivalta et al. 2019, Buono et al. 2025), ~~past vent positions may track the~~and producing mostly lateral propagation with trajectories ~~of~~controlled by the ~~dykes that fed those eruptions. The centre can be approximately assumed at the point~~structure of ~~maximum deformation, representing~~ the ~~centre of~~caldera and the ~~bell-shaped deformation of Campi Flegrei~~consequent stress field. ~~Here, it is set to LON 4263554 and LAT 451954 (UTM WGS84, zone 33N),~~

Assuming a magma origin located around the centre of the caldera, independently of its specific depth and geometry, the empirical track of these features may be retrieved by studying the distribution of past vents around the caldera centre. These empirical distributions can then be used to set a vent opening probability map. The probability density function in a specific point in the caldera can be calculated in polar coordinates using the following formula:¶

$$f_{pol}(r,\theta) = f_r(r) f_\theta(\theta). \quad (1)$$¶

where the term $f_r(r)$ is the probability distribution for the distances from the centre of the caldera and the term $f_\theta(\theta)$ is the angular probability distribution. In this formulation, it is assumed that these two distributions can be considered independent. Indeed, the physical process described in Rivalta et al. (2019) suggests a potential independence between direction of dyke propagation and distance from the caldera centre, as they are controlled by two different features of the caldera, being the distance fundamentally controlled by the size of the nearly circular shape of the caldera, and the direction predominantly controlled by local topographic features. This independence should also leave an empirical track in past vent positions, which can also be formally verified by testing whether the direction and the distances found using past vent positions are correlated to each other.¶

The probability distribution of eq. (1) can be transformed into Cartesian coordinates as follows:¶

$$f_{xy}(x,y) = \frac{1}{r} f_{pol}(r,\theta) = \frac{1}{r} f_r(r) f_\theta(\theta) \quad . \quad (2)$$¶

where the term $f_{pol}(r,\theta)$ is again factorized in its two terms using Eq. (1). Defining an application grid, equation (2) can be used to establish a vent probability map by substituting $f_r(r)$ and $f_\theta(\theta)$ with the appropriate distributions of potential distance-from-centre and azimuth. Depending on the available data, such distributions may be estimated empirically, looking at the distribution of past vents, including all the data that reflect the present state the caldera, or analyzing the topographical peaks surrounding the caldera. ¶

3. Results¶

The position of the caldera centre is here assumed at the point of maximum uplift, here set 800 meters south of the GNSS station of Rite at coordinates LON 426355 and LAT 4518743 (UTM WGS84, zone 33N; Bevilacqua et al., 2024, Fig. 1). ¶

~~Based on this, it is possible to~~To establish an empirical model~~ for such trajectories by studying~~, we study the empirical distribution of azimuth (angle to the North of the line connecting the centre of the caldera and the vent, hereinafter angle or azimuth) and distance-from-the-centre of the caldera (hereinafter ~~radius~~distance) of past eruptions. We consider the ~~caldera~~71 vent positions of the ~~dykes that alimented past eruptions, and use this model to define a forecast map for future vents~~post-NYT activity (Bevilacqua et al. 2016). Past vent positions are~~ however~~ affected by significant uncertainty. To ~~account for this~~evaluate their potential impact all statistical analyses, we ~~used~~consider the ~~71 vent positions and corresponding~~ uncertainty bounds defined in Bevilacqua et al. (~~2015~~2016), accounting for the uncertainty by randomly sampling 1000 alternative synthetic positions uniformly distributed within the defined uncertainty bounds (Supplementary Figure 1).

¶

~~2~~3.1 ~~Length~~Empirical distributions of ~~dyke propagation~~distance and azimuth

¶

~~At~~We first~~, we~~ analyse the distances between the centre of the caldera and all post-NYT vents. Under the assumption of propagation from the caldera centre, ~~which represent~~this distance represents the length of the horizontal propagation of the dykes that alimented such eruptions. The analysis is conducted separately for the three epochs~~, and jointly for the entire dataset~~. For simplicity, the recent Monte Nuovo eruption is included in the third epoch. In Figure ~~1A~~2A, we report the empirical distributions (histograms with bins of 250 m, the corresponding empirical cumulative distribution functions are reported in Supplementary Figure 2), revealing a strong difference between the first epoch, where 60% of eruptions occur between 4,400 and 6,600 m, and the third epoch that shows shorter distances, with two significant peaks around 4,000 m and 2,000 m, being Epoch 2 somehow intermediate between the other~~ two. A~~ two~~-sample Kolmogorov-Smirnov test (KS2) confirms that this difference is statistically significant also accounting for vent position uncertainty (significance level of 0~~.01, Supplementary Figure 3), confirming the already observed progressive inward migration of post-NYT volcanism (Di Vito et al. 1999; Orsi et al. 2004; Isaia et al. 2009; Rivalta et al. 2019).~~

~~2~~To test if the distributions for the different Epochs are different, we implement a two-sample Kolmogorov-Smirnov test (KS2), a non-parametric statistical test used to determine if two independent datasets are drawn from the same underlying distribution (Gibbons and Chakraborti, 2003). Here and in the following tests, the significance level (red line) is set to 0.01 and it is corrected for multiple testing using the Bonferroni (1936) criterion, which consists of dividing the significance level by the number of comparisons.~~2 Direction~~ The test confirms that the difference between Epoch 1 and Epoch 3 is statistically significant also accounting for vent position uncertainty (see Supplementary Figure 3), confirming the already observed progressive inward migration of ~~dykes propagation~~post-NYT volcanism (Rivalta et al. 2019).

~~The~~Following Rivalta et al. (2019), under the assumption of propagation from the caldera centre, the direction of propagation of the dykes~~, which~~ is ~~instead~~ controlled by topographic asymmetries~~,~~. This direction can be investigated by ~~analyzing~~analysing the azimuth of ~~the propagation~~past vents with respect to the centre of the caldera~~, parameterized as the angle to the North of the line connecting the centre of the caldera and the vent~~. In Figure ~~1B~~2B, we report the empirical distributions for the different epochs (histogram with bins of 20 degrees, the corresponding empirical cumulative distribution functions are reported in Supplementary Figure 2), showing that most of eruptions have an azimuth ~~around~~ toward NE (50°, toward Astroni, Agnano, and ~~no~~Solfatara). No specific differences between the distributions are visible. This observation is tested again with a two-sample Kolmogorov-Smirnov test (~~s.l. 0.01,~~ see Supplementary Figure 3), confirming that the directions of dyke propagation are similar in all epochs~~, with a primary peak toward NE (50°, toward Astroni, Agnano, and Solfatara)~~.

¶

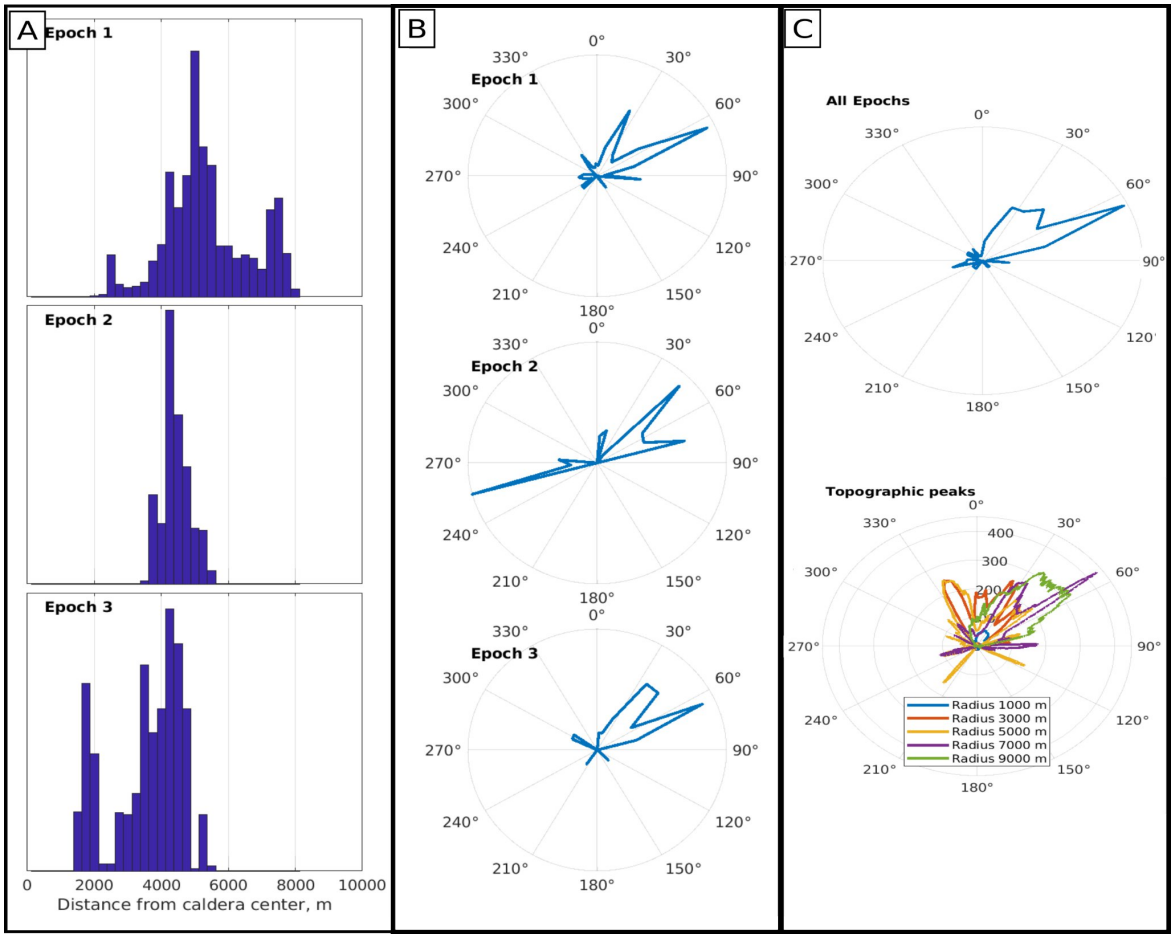
A
Epoch 1
Epoch 2
Epoch 3
0
2000
4000
6000
8000
10000
Distance from caldera center, m
B
Epoch 1
Epoch 2
Epoch 3
0°
30°
60°
90°
120°
150°
180°
210°
240°
270°
300°
330°
C
All Epochs
Topographic peaks
400
300
200
Radius 1000 m
Radius 3000 m
Radius 5000 m
Radius 7000 m
Radius 9000 m

150

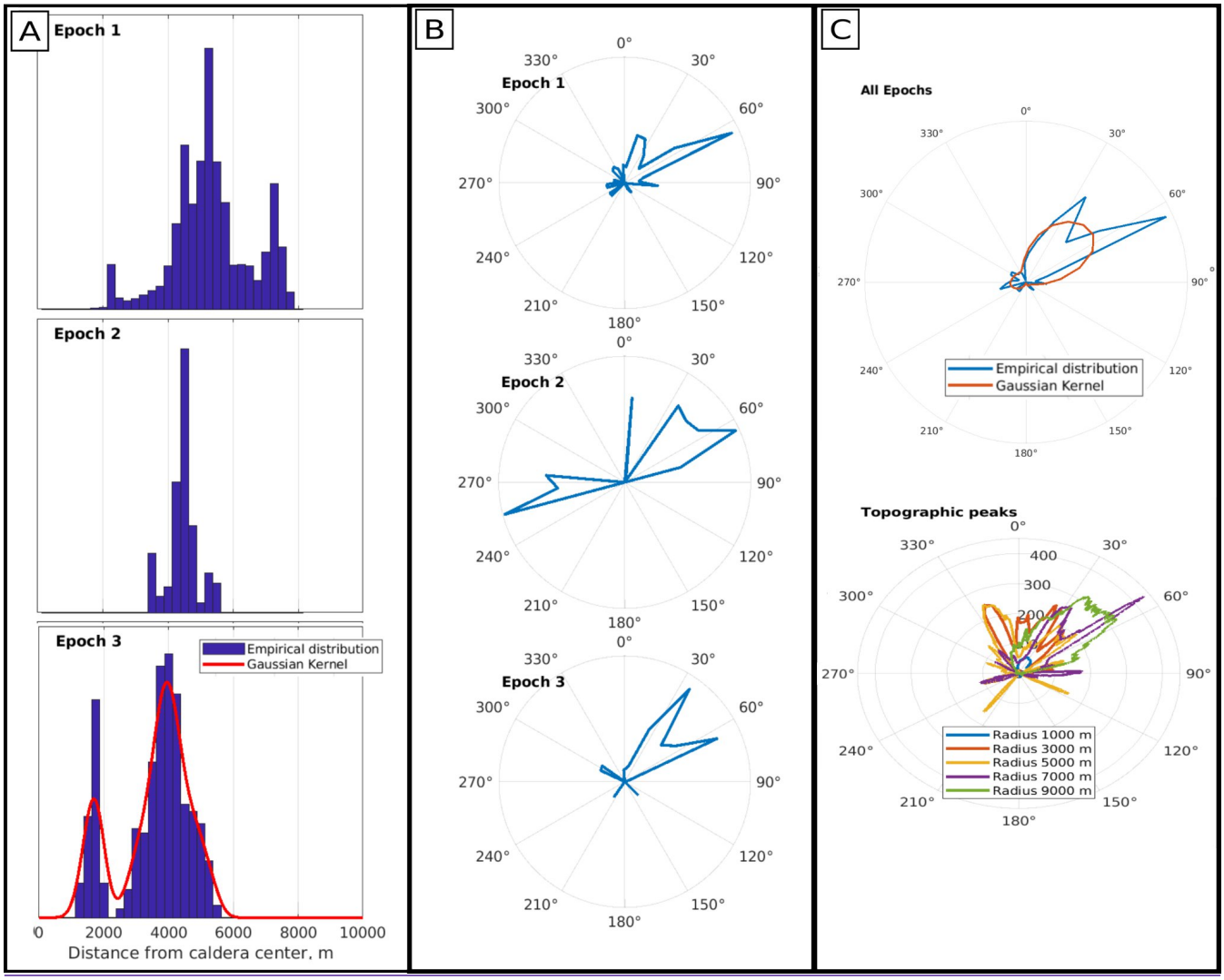

Figure ~~12~~: (A) Empirical distribution of distances from the ~~center~~centre of the caldera (dyke propagation length) for Epochs 1, 2 and 3. The red line in Epoch 3 reports a Gaussian kernel smoothing the empirical distribution. (B) Empirical distribution of azimuth (dyke direction) for Epochs 1, 2 and 3. (C) Empirical distribution of azimuth (dyke direction) for all Epochs (the red line in Epoch 3 reports a Gaussian kernel smoothing the empirical distribution) and ~~azimuth~~the maxima of topographic peaks in radial swaths of variable length from the caldera centre.

¶

¶

Rivalta et al. (2019) suggest that preferential directions may be induced by topographic peaks that locally modify the stress field, which is mainly controlled by unloading. To investigate this empirically, we analyse the maxima of the topography surrounding the caldera, retrieving the maxima in all directions ~~within a given maximum~~in swaths with different length, hereinafter called radius. Maximum radii from ~~2~~1 to ~~10~~9 km are tested: for each radius, the distribution of topographic maxima as a function of azimuth is normalised and compared with the azimuthal distribution of past eruptions (Figure ~~1C~~2C). For

simplicity, the present day topography is adopted, even if some of the edifices (and the corresponding topographic peaks) were built during the post-NYT activity. The comparison confirms the correlation anticipated by Rivalta et al. (2019). The primary peak is NE (around 50°) corresponds to the topographic peak associated with La Starza marine terrace (Fig. 1, for a radius of 1 km) and Camaldoli Hill (for radii of 3 km and larger). In agreement with Rivalta et al. (2019), the latter topographic peak is the most pronounced and it coincides with the highest concentration of eruptive vents during various eruptive periods. A secondary peak appears in the NNW direction (~~-45~~around 330°) for intermediate radii ~~larger than~~(between 3 and 5 km), corresponding to the peak of the Gauro volcanic edifice (Monte Barbaro): this edifice was created during one of the first eruptions of the first epoch, and does not correspond to any peak in the observed distribution of azimuth. However, this secondary peak becomes less important for large radii (7 km and above), due to the Camaldoli Hill. Performing a Kolmogorov-Smirnov test between the angular distributions of past vents and of topographic peaks, the largest p-values correspond to a maximum distance of 7 km~~, which is the only case for which the~~. The null hypothesis of equal distribution is consistently not rejected independently from vent position uncertainty ~~(s.l. 0.01~~only for radii of 7 and 9 km, while it is rejected for smaller radii (Supplementary Figure 4).

~~3 Vent opening probability~~¶

~~The empirical distributions obtained in Section~~ 3.2 ~~can be used to set a vent~~Vent opening probability ~~map. The probability density function in a specific point in the caldera can be calculated in polar coordinates using the following formula:~~for Campi Flegrei

~~$$f_{pol}(r,\theta) = f_r(r) f_\theta(\theta). \quad (1)$$~~¶

~~where~~To apply Eq. (2) and quantify the ~~term $f_\theta(\theta)$ is the angular~~vent probability ~~distribution~~map, we first test the independence of the ~~term $f_r(r)$ is~~radial and the ~~probability distribution for~~azimuth distributions, by testing whether the ~~distances from~~direction and the ~~center~~distances of ~~the caldera~~past vent positions are correlated to each other. ~~In~~To this ~~formulation~~end, we divide the directions in the 4 sectors (SW, NW, NE, ~~it is assumed that these two distributions can be considered independent~~and SE), ~~being~~and we compare the ~~latter fundamentally controlled by~~distribution of distances in the ~~nearly circular shape of~~different sectors again using the ~~caldera and~~Kolmogorov-Smirnov test. All the ~~former predominantly controlled by local topographic features~~six couples are tested. ~~This probability~~The results (see Supplementary Figure 6) show that the hypothesis of equal distribution ~~can~~cannot be ~~transformed into Cartesian coordinates as follows:~~rejected for all combinations of sectors, standing for the independence of the two parameters.

¶

~~$$f_{xy}(x,y) = \frac{1}{r} f_{pol}(r,\theta) = \frac{1}{r} f_r(r) f_\theta(\theta) \quad . \quad (2)$$~~¶

~~where the term $f_{pol}(r,\theta)$ is factorized in its two independent terms.~~ ¶

To develop the probability map, we define a grid 14.5 x 12.5 km, ~~centered~~centred at LON 427406 and LAT 4518958 (UTM WGS 84 33N), with 700 square cells 500 x 500 m, equal to the one adopted in Selva et al. (2012).~~-~~ Then, the probability in each cell ~~can be~~is computed by numerically integrating ~~$f_{xy}(x,y)$~~$f_{xy}(x,y)$ computed through Eq. (2), where the terms ~~$f_r(r)$~~$f_r(r)$ and ~~$f_\theta(\theta)$~~$f_\theta(\theta)$ can be set using the empirical distributions developed in Section ~~2~~3.1.

In particular, we propose 2 alternative implementations. At first, we consider for both ~~$f_r(r)$~~$f_r(r)$ and ~~$f_\theta(\theta)$~~$f_\theta(\theta)$ the empirical distributions that may be considered representatives of the present state of the caldera. Hereinafter, this first approach is referred to as model M1. To generalize the empirical distributions, we apply Gaussian kernels (red curves in Fig. 2A,C). The most appropriate bandwidth is defined using a leave-one-out technique with a Kullback-Leiber score (Connor et al. 2019). In particular, we set ~~$f_r(r)$~~$f_r(r)$ as the radial distribution of the eruptions of Epoch 3 (including also Monte Nuovo), ~~which is indeed~~i.e. the most recent ~~and~~. As Epoch 1 is significantly different ~~from~~for the ~~one~~distribution of distances, its consideration would introduce a bias for forecasting future behaviours. Here, being very close in time to Epoch 1, Epoch 2 is assimilated to it, and only Epoch 3 is considered. The distribution is also truncated at 10 km, where it essentially the ~~previous epochs~~distribution drops to 0 (red line in Fig. 1A). The more appropriate bandwidth is found to be 275 m (Supplementary Figure 6a). ~~Then~~To set $f_\theta(\theta)$, we ~~set $f_\theta(\theta)$ as~~instead consider the ~~azimuthal~~azimuth distribution of all post-NYT eruptions (red line in Fig 1C), as the different epochs are statistically indistinguishable~~. The result is reported in Figure 2A~~. ~~A second implementation is also tested by substituting~~For the ~~empirical azimuthal distribution with the distribution of the topographic maxima for a radius of 7,000 m~~kernel, the ~~one that better correlates with past vents. The results are reported in~~more appropriate bandwidth is found to be 17 degrees (Supplementary Figure ~~2B~~6b). ~~The numerical values for both models are reported as Supplementary File.~~

A second implementation is also tested by setting $f_\theta(\theta)$ differently, that is by substituting the empirical azimuth distribution adopted in M1 with the distribution of the topographic maxima for a radius of 7,000 m, the one that better correlates with past vents. Hereinafter, this second approach is referred to as model M2.¶

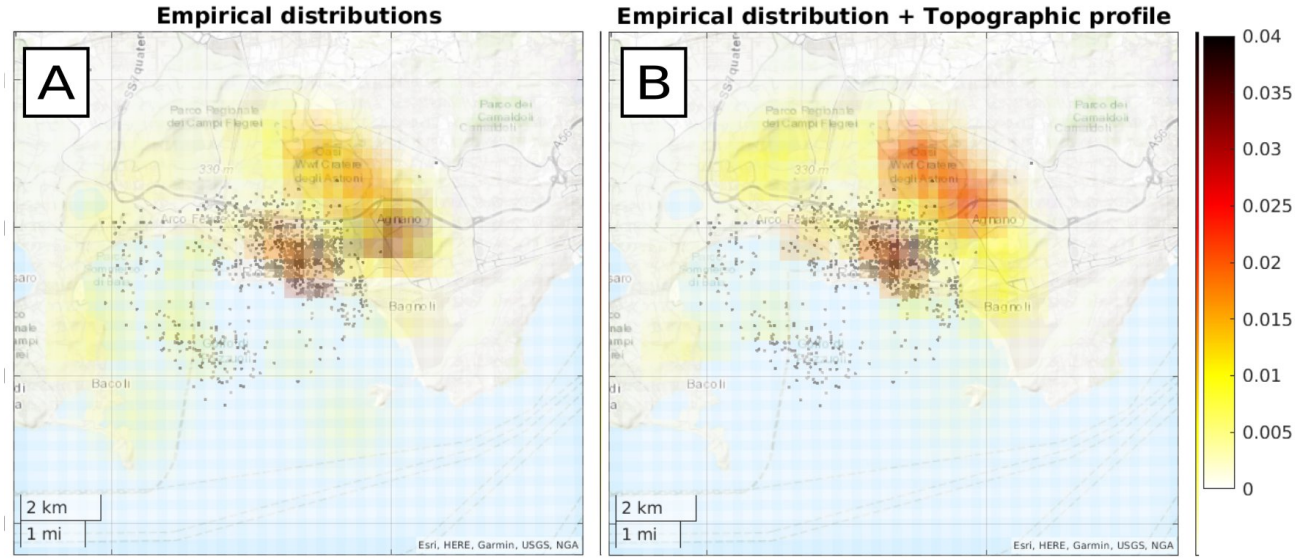

The results of the two alternative implementations M1 and M2 are reported in Figure 3. The numerical values for both models are reported as Supplementary File.

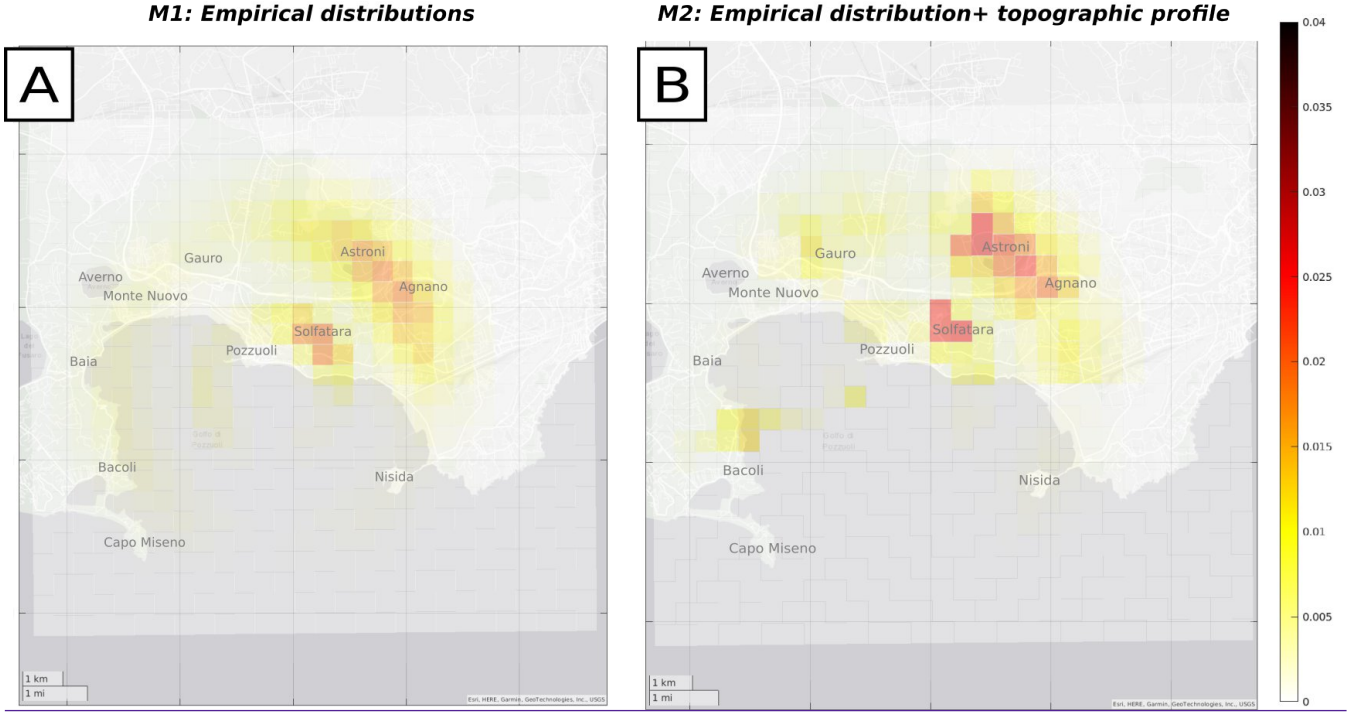

Figure ~~23~~: Vent opening probability maps: (A) model M1, based empirical distances and azimuth, (B) model M2, based on empirical distances and topographic azimuth~~. Black dots indicate seismicity (Md > 1.0) in the period June 2023 - June 2025.~~

¶

4. Discussion

The ~~two probability~~resulting maps ~~in Figure 2~~ are similar, with two distinct probability peaks in the NE direction at about 4 and 2 km from the ~~center~~centre, corresponding to the Agnano-Astroni and the Solfatara area, respectively. ~~Considering~~In M2, which considers the topographic contribution (Figure 3B), the angular probability values are ~~more distributed~~less smoothed than ~~when~~in model M1, where the empirical distributions ~~is considered~~are smoothed by the kernels (Figure 3A). The effect is that the maximum probability values in the area at ~~NW~~NE is almost halved~~. The~~ in M1; also the relative peaks in the other directions appear relatively more evident ~~when only empirical distributions are considered, generating two concentric and separated rings at about 2 and 4 km~~in M2, with secondary peaks ~~also~~ in the submerged side of the caldera toward ~~the E and SE~~W, in the direction of ~~Baia and~~ Bacoli, as well as the inland area toward NNW. On the contrary, in M1 probabilities are more distributed, generating two concentric and separated rings of larger probabilities at 2 and 4 km from the caldera centre.

Comparing these results with the main probability maps for Campi Flegrei discussed in the literature - Alberico et al. (2002), Selva et al. (2012), and Bevilacqua et al. (2015), hereinafter indicated as A02, S12 and B15, respectively - interesting coincidences and some significant differences emerge. ~~The~~As already noted, the map produced by ~~Alberico et al. (2002)~~A02 differs widely from ~~all others~~S12 and B15 maps, having maximum values in the ~~center~~centre of the caldera ~~and close to 0 in the peripheral areas~~, which is in contrast with the empirical evidence~~. The higher probability areas~~ of ~~Selva et al~~recent past vents. ~~(2012)~~In this, M1 and ~~Bevilacqua et al (2015) (Figure 3A-B), such as the Agnano area~~M2 are closer to ~~the NE of the caldera, coincide with those identified here. The two peaks at distances of 2~~S12 and ~~4 km from the caldera center are in the range forecasted by Rivalta et al. (2019) when adopting only Epoch III data (Figure 3C). All these salient features are indeed present in all studies~~B15, ~~as they essentially correspond~~providing lower probabilities close to the ~~spatial distribution of past vents. However, there are also some significant differences. The propagation distance distribution here produces two distinct peaks at 2~~caldera centre and ~~4 km, more than a continuous distribution~~larger probabilities in ~~this range, generating two distinct rings at relatively higher probability. In~~ the ~~areas~~NE area of ~~Nisida~~Astroni and ~~Campo Miseno~~Agnano, ~~the probability values obtained here are relatively lower than in literature studies. The secondary peak identified in the Averno area in Selva et al., (2012) appears only in the map based on topography, but it is significantly shifted eastward, in the direction~~where most of ~~the Gauro, due to its topographical peak~~past vents concentrate.

To better highlight further similarities and differences, in Figure 4A-F we report the maps of the relative differences in probability between M1, M2 and A02, S12, and B15, rescaling all of them to the same grid and, for S12 and B15, considering the mean of the epistemic uncertainty (Supplementary Figure 7). These maps highlight that the main differences are connected to the two rings discussed above, which were not present in previous studies. ¶

The outer ring, at 4 km, coincides with the area identified by Charlton et al. (2020), and includes the higher probability area of S12 and B15, located in the Agnano area to the NE of the caldera. However, also in this area, both M1 and M2 provide larger probabilities (panels B, C, E, F). This ring also includes the area of Monte Nuovo (N, last eruption at Campi Flegrei), and especially M1 provides larger probabilities than previous studies. Also the secondary peak identified in the Averno area (NW) in S12 is found in M1 and M2, but shifted inward and eastward, in the direction of Gauro. ¶

257

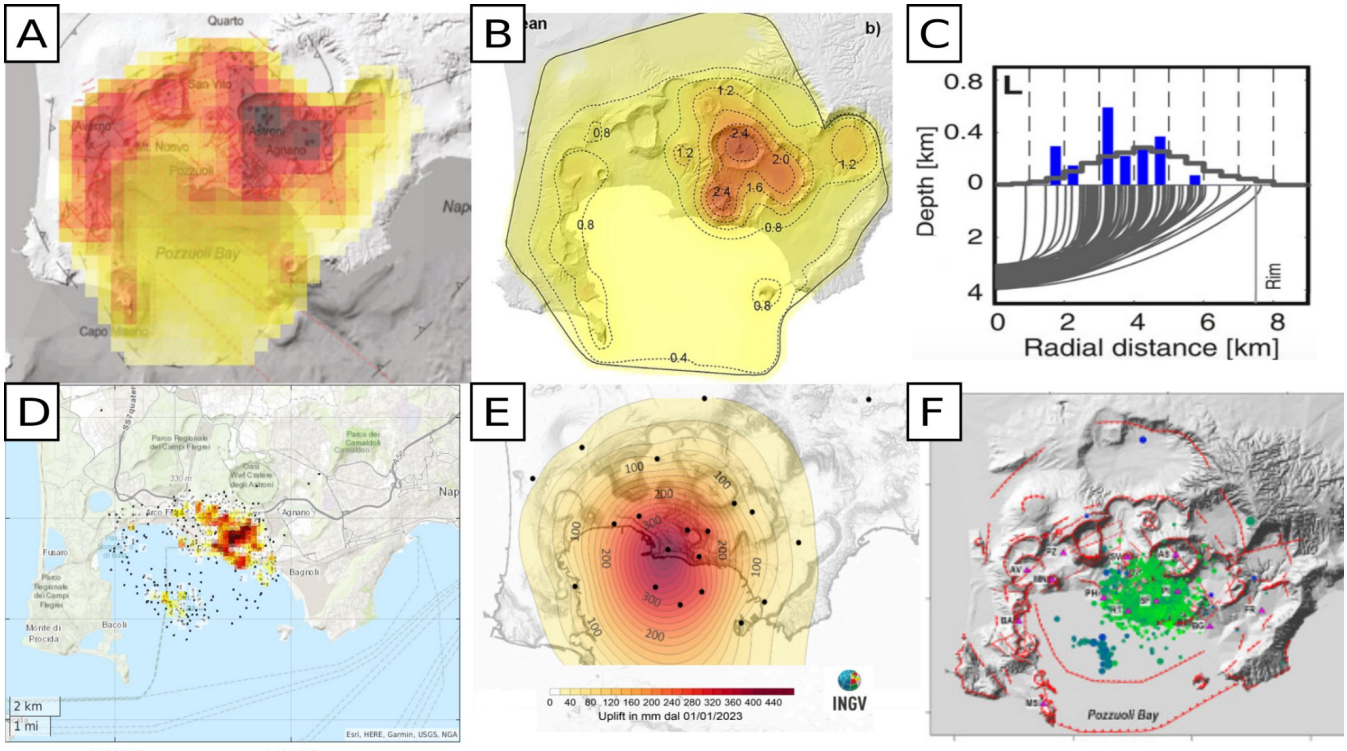
A
Quarto
San Vito
Astroni
Agnano
Pozzuoli
Pozzuoli Bay
Capo Miseno
B
b)
1.2
0.8
2.4
2.0
1.6
0.4
C
L
Depth [km]
0.8
0.4
0
2
4
Rim
0
2
4
6
8
Radial distance [km]
D
Parco Regionale dei Campi Flegrei
Agnano
Fusaro
Bagnoli
Monte di Procida
Baia
2 km
1 mi
Esri, HERE, Garmin, USGS, NGA
E
100
200
300
0 40 80 120 160 200 240 280 320 360 400 440
Uplift in mm dal 01/01/2023
INGV
F
Pozzuoli Bay

258

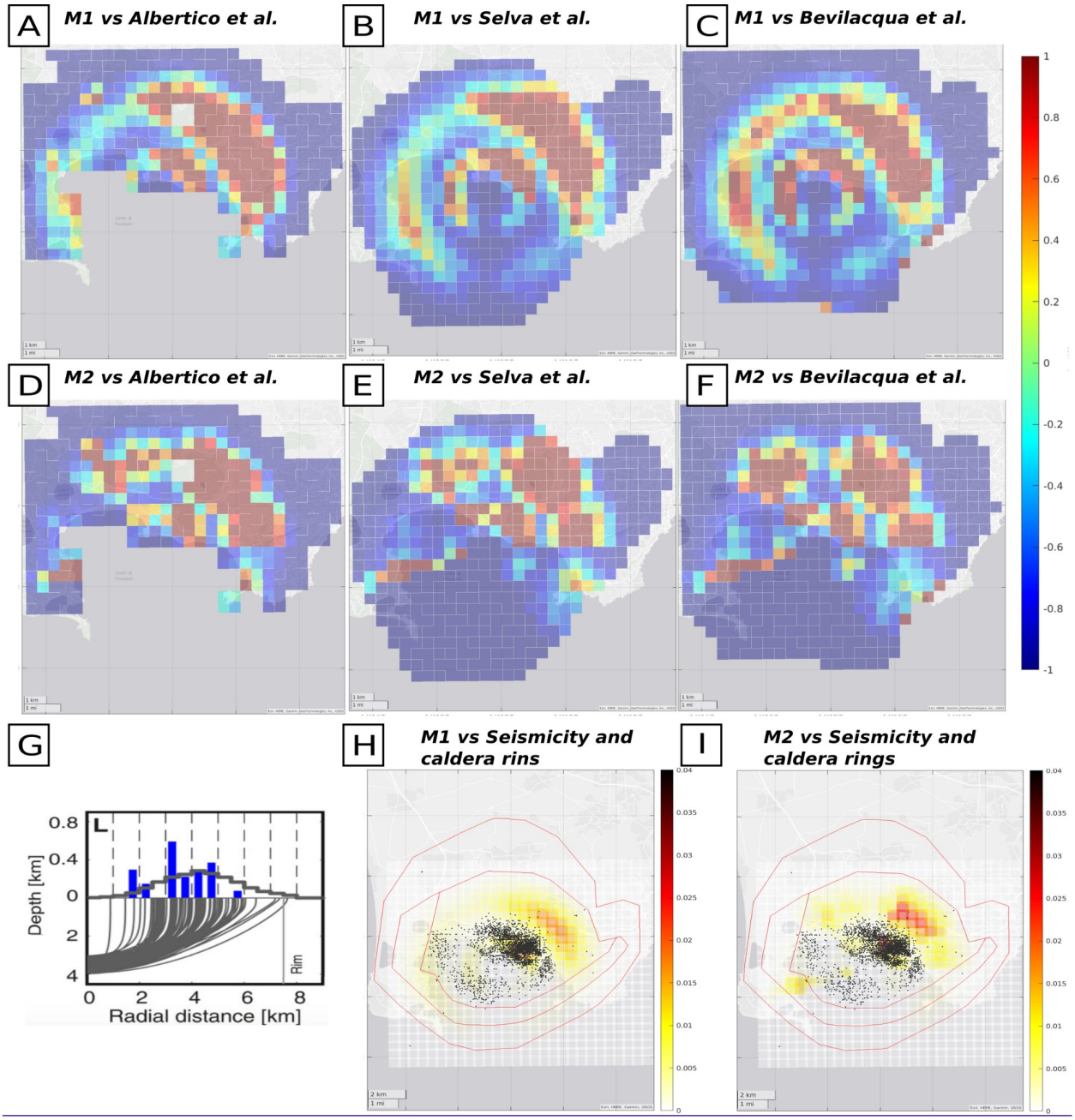

Figure ~~34~~: Relative difference between (A) ~~**Vent opening probability maps form**~~M1 and Albertico et al. (2002), (B) M2 and Alberico et al. (2002), (C) M1 and Selva et al. (2012), (D) M2 and Selva et al. (2012), (E) M1 and Bevilacqua et al. (~~**B**~~2015), (F) ~~**Vent opening probability map from**~~M2 and Bevilacqua et al. (2015). Positive numbers mean that M1/M2 are larger than literature studies. (~~**C**~~G) Forecasted distances from the ~~**center**~~centre of the caldera from Rivalta et al. (2019) ~~**(D) Spatial density.**~~ Comparison between the spatial distribution of Campi Flegrei seismicity (Md > ~~1~~0.5) in the period June 2023 - June 2025~~.~~, the

caldera rims (~~E) uplift~~as mapped in ~~the period January 2023 - June~~Natale et al. 2024, 2025 ~~(modified from Osservatorio Vesuviano 2025~~). ~~(F) 2011–2022 seismicity (green circles),~~ and ~~main structural features~~M1 (~~magenta lines~~panel H)~~: outcropping faults, the Campanian Ignimbrite~~ and ~~Neapolitan Yellow Tuff caldera borders and outer/inner rims~~M2 (~~modified from Tizzani et al 2024~~panel I).

¶

¶

The outer ring also generates several other secondary probability peaks at sea in the W directions, in the direction of the topographic peaks of Baia/Bacoli, especially in M1, These peaks are larger than in literature maps. On the other hand, in the areas of Nisida (SE) and Capo Miseno (SW), the probability values obtained here are relatively lower than the ones in literature. ¶

The inner ring includes the high probability area of Solfatara, present in both S12 and B15, but also in this case both M1 and M2 provide larger probabilities (Fig. 4B, C, E, F). In addition, the inner ring introduces new peaks in probability within the bay, toward W, and in the coastal area of La Starza, toward E, both less pronounced in previous studies. ¶

Also in the outer area of the caldera, external to the outer ring, M1 and M2 are different than previous studies. Here, M1 and M2 do not assume that vent opening may occur only inside the caldera border, as in S12 and B15, but an outer limit is established by the maximum observed distance from the centre of the caldera in Epoch 3 (Section 3.1). This cuts out the most external areas, mainly toward E, NW and S, where both M1 and M2 foreseen smaller probabilities than previous models. ¶

¶

5. Conclusions ¶

~~Also~~The vent opening maps derived in the paper are based on assumptions radically different from the ~~probability peak at Solfatara, which is found~~ones in ~~both maps produced here,~~literature. The approach is ~~more evident here than~~inspired from the dyke propagation model proposed in ~~literature studies~~Rivalta et al. ~~This is~~(2019), which suggests a ~~consequence~~substantial independence between the radial and azimuthal distributions of dykes propagating from the centre of ~~combining~~the caldera. The results confirm some of the ~~peaks~~features already highlighted in ~~distance and angles~~previous studies, but also it introduces important differences. ~~This effect~~In particular, the most striking difference is ~~also evident in~~that the ~~other secondary~~vent probability peaks in two circles at ~~sea~~around 2 and 4 km from the caldera centre, with significant modulations in the ~~E and SE~~different directions, while smaller probabilities are found in the ~~direction~~peripheral areas of the ~~topographic peaks of Baia and Capo Miseno~~caldera. These ~~peaks emerge here~~rings, particularly evident in model M1 but ~~they were not found~~present also in model M2, are compatible with in ~~literature studies~~the range forecasted by Rivalta et al. (2019) when adopting only Epoch 3 data (Fig. 4G). However, the propagation distance distribution here produces two distinct peaks at 2 and ~~they~~4 km, more than a continuous distribution in this range. The inner circle essentially ~~coincide~~coincides with ~~one spot of~~an area characterized by high seismic activity recorded in the ongoing unrest episode (black dots in Fig. ~~3D~~4H,I), ~~as well as in~~while the ~~past monitored unrest episodes. In particular, in Fig. 3D, we report~~outer circle is instead closer to the the ~~spatial density~~position of the ring faults surrounding the ~~seismicity recorded~~inner caldera (red lines in ~~the last two years~~Fig. 4H-I, Natale et al. 2024, ~~which shows a striking correspondence~~2025). These observations are completely independent and seem to

spot privileged paths for magma ascent around the ~~vent probability maps reported in Fig~~inner caldera border. ~~2A~~This may be the subject of future studies.

~~More in general,~~It is important to stress that M1 and M2 are produced using the ~~two higher probability rings~~empirical distributions which are considered relevant for forecasting future occurrences, that ~~emerge here correspond to~~is Epoch 3 for distances, and either all epochs or topographic peaks for angles. Indeed, while the distribution of the azimuth does not change significantly across epochs, the ~~position~~analysis of the ~~ring faults surrounding~~distances with respect to the ~~inner~~centre of the caldera ~~and bordering~~has shown that Epoch 1 differs significantly from Epoch 3 in terms of distances. This confirms the ~~area~~findings of ~~maximum uplift (Fig 3D and 3F, Tizzani~~Rivalta et al. ~~2024~~(2019), ~~Natale~~and it is in agreement with Orsi et al. ~~2025~~(2004)~~. These observations are completely independent~~, who concluded that the last change in stress regime occurred prior to onset of the Epoch 3, and ~~may help spotting privileged paths~~suggested that only the past 5 ka should be considered as reference for ~~magma ascent around~~the present state of the ~~NYT~~ caldera ~~border~~(Orsi et al. 2009). This assumption was adopted also in Selva et al. (2012).

Finally, even if here we develop two maps, we prefer not to quantify the epistemic uncertainty on the proposed approach, differently from what was done in previous studies like Selva et al. (2012) and Bevilacqua et al (2015). The reason is that several case studies recently demonstrated that the effective epistemic uncertainty on a target physical process (here vent opening) is better estimated by combining radically alternative approaches (e.g., defining weighted ensembles of alternative¶ models), rather than by exploring the epistemic uncertainty inherent to one specific approach (Selva et al. 2015; Marzocchi et al. 2021; Meletti et al. 2021, among the others). Consequently, while the epistemic uncertainty on a given approach may be of relative interest, the very development of an alternative approach like the one presented here may be a significant added value to future quantification of epistemic uncertainty in the process of vent opening at Campi Flegrei, via multi-model ensembles or equivalent approaches that combine all the scientifically grounded approaches available in literature (e.g. SSHAC 1997, Marzocchi et al. 2017, 2021).¶

¶

Datasets

The position of the vents related to past eruptions was obtained from Bevilacqua et al. (2015). The DEM ~~of the area obtained from~~used to find topographic peaks around Campi Flegrei is TINITALY (Tarquini et al. 2023) with WGS 84 / UTM zone 33N coordinates, available at https://tinitaly.pi.ingv.it/.

Author contributions¶

JS and NM conceived and developed the Methodology. JS supervised the project. NM implemented the preliminary software for the analyses, with the support of JS. JS finalized the software and prepared the original draft. All the authors reviewed and approved the manuscript. ¶

¶

~~Acknowledgements~~Acknowledgments

The figures and maps have been produced using Matlab and/or InkScape software.

¶

References

Alberico, I., Lirer, L., Petrosino, P., & Scandone, R. (2002). A methodology for the evaluation of long-term volcanic risk from pyroclastic flows in Campi Flegrei (Italy). Journal of Volcanology and Geothermal Research, 116, 63–78. https://doi.org/10.1016/S0377-0273(02)00211-1

Amoruso, A., Crescentini, L., Sabbetta, I., De Martino, P., Obrizzo, F., & Tammaro, U. (2014). Clues to the cause of the 2011–2013 Campi Flegrei caldera unrest, Italy, from continuous GPS data. Geophysical Research Letters, 41, 1–7. https://doi.org/10.1002/2014GL059539

Barberi, F., Corrado, G., Innocenti, F., & Luongo, G. (1984). Phlegraean fields 1982–1984: Brief chronicle of a volcano emergency in a densely populated area. Bulletin of Volcanology, 47, 175–185. https://doi.org/10.1007/BF01961547

Bevilacqua, A., Isaia, R., Neri, A., Vitale, S., Aspinali, W. P., Bisson, M., Flandoli, F., Baxter, P. J., Bertagnini, A., Ongaro, T. E., Iannuzzi, E., Pistolesi, M., & Rosi, M. (2015). Quantifying volcanic hazard at Campi Flegrei caldera (Italy) with uncertainty assessment: 1. Vent opening maps. Journal of Geophysical Research: Solid Earth, 120, 2309–2329. ~~https://doi.org/10.1002/2014JB011775~~https://doi.org/10.1002/2014JB011775

¶

Bevilacqua A, Flandoli F, Neri A, Isaia R, Vitale S (2016). Temporal models for the episodic volcanism of Campi Flegrei caldera (Italy) with uncertainty quantification. J Geophys Res Solid Earth 121:7821–7845. ¶
https://doi.org/10.1002/2016JB013171¶

¶

Bevilacqua, A., Neri, A., De Martino, P. et al. (2024) Accelerating upper crustal deformation and seismicity of Campi Flegrei caldera (Italy), during the 2000–2023 unrest. Commun Earth Environ 5, 742.¶
https://doi.org/10.1038/s43247-024-01865-y¶

Bevilacqua, A., Neri, A., De Martino, P. et al. (2024). Accelerating upper crustal deformation and seismicity of Campi Flegrei caldera (Italy), during the 2000–2023 unrest. Commun Earth Environ 5, 742. https://doi.org/10.1038/s43247-024-01865-y

¶

Bonferroni C., 1936. Teoria statistica delle classi e calcolo delle probabilità. Pubblicazioni del Regio Istituto Superiore di Scienze Economiche e Commerciali di Firenze, 8, 3–62. (in Italian).¶

Buono, G., Paonita, A., Pappalardo, L., Caliro, S., Tramelli, A., & Chiodini, G. (2022). New insights into the recent magma dynamics under Campi Flegrei caldera (Italy) from petrological and geochemical evidence. Journal of Geophysical Research: Solid Earth, 127, e2021JB023773. https://doi.org/10.1029/2021JB023773

Buono, G., Maccaferri, F., Pappalardo, L., Tramelli, A., Caliro, S., Chiodini, S., Pinel, V., Rivalta, E., Spagnuolo, E., Trasatti, E., Di Vito, M.A. (2025). Weak Crust Owing Past Magmatic Intrusions Beneath Campi Flegrei Identified: The Engine for Bradyseismic Movements? AGU Advances, 6, e2024AV001611. https://doi.org/10.1029/2024AV001611

Charlton, D., Kilburn, C., & Edwards, S. (2020). Volcanic unrest scenarios and impact assessment at Campi Flegrei caldera, Southern Italy. Journal of Applied Volcanology, 9(7). https://doi.org/10.1186/s13617-020-00097-x

Chiodini, G., et al. (2021). Hydrothermal pressure–temperature control on CO_2 emissions and seismicity at Campi Flegrei (Italy). Journal of Volcanology and Geothermal Research, 414, 107245. https://doi.org/10.1016/j.jvolgeores.2021.107245

D'Antonio, M., Tonarini, S., Arienzo, I., Civetta, L., & Di Renzo, V. (2007). Components and processes in the magma genesis of the Phlegrean Volcanic District (Southern Italy). In L. Beccaluva, G. Bianchini, & M. Wilson (Eds.), Cenozoic volcanism in the Mediterranean area (pp. 203–220). Geological Society of America Special Paper 418.

Del Gaudio, C., Aquino, I., Ricciardi, G. P., Ricco, C., & Scandone, R. (2010). Unrest episodes at Campi Flegrei: A reconstruction of vertical ground movements during 1905–2009. Journal of Volcanology and Geothermal Research, 195, 48–56. https://doi.org/10.1016/j.jvolgeores.2010.02.002

Di Vito, M. A., Acocella, V., Aiello, G., Barra, D., Battaglia, M., Carandente, A., Del Gaudio, C., De Vita, S., Ricciardi, G. P., Ricco, C., Scandone, R., & Terrasi, F. (2016). Magma transfer at Campi Flegrei caldera (Italy) before the 1538 AD eruption. *Scientific Reports*, *6*, 32245. https://doi.org/10.1038/srep32245

Di Vito, M. A., Isaia, R., Orsi, G., Southon, J., de Vita, S., D'Antonio, M., Pappalardo, L., & Piochi, M. (1999). Volcanism and deformation since 12,000 years at the Campi Flegrei caldera (Italy). Journal of Volcanology and Geothermal Research, 91(2–4), 221–246. https://doi.org/10.1016/S0377-0273(99)00037-2

Fernandez, G., Giaccio, B., Costa, A., Monaco, L., Nomade, S., Albert, P. G., Pereira, A., Flynn, M., Leicher, N., Lucchi, F., Petrosino, P., Palladino, D. M., Milia, A., Insinga, D. D., Wulf, S., Kearney, R., Veres, D., Jordanova, D., Putignano, M. L., Isaia, R., & Sottili, G. (2024). New constraints on the Middle–Late Pleistocene Campi Flegrei explosive activity and

Mediterranean tephrostratigraphy (~160 ka and 110–90 ka). *Quaternary Science Reviews*, *331*, Article 108623. https://doi.org/10.1016/j.quascirev.2024.108623¶

¶

Gibbons, J. D., and S. Chakraborti (2003), Non-parametric Statistical Inference, 4th ed., 645 pp., Marcel Dekker, New York¶

Giudicepietro, F., Avino, R., Bellucci Sessa, E., et al. (2025). Burst-like swarms in the Campi Flegrei caldera accelerating unrest from 2021 to 2024. Nature Communications, 16, 1548. https://doi.org/10.1038/s41467-025-56723-y

Isaia, R., Marianelli, P., & Sbrana, A. (2009). Caldera unrest prior to intense volcanism in Campi Flegrei (Italy) at 4.0 ka B.P.: Implications for caldera dynamics and future eruptive scenarios. Geophysical Research Letters, 36, L06304. https://doi.org/10.1029/2008GL036962

¶

Isaia, R., Vitale, S., Marturano, A., Aiello, G., Barra, D., Ciarcia, S., Iannuzzi, E., & Tramparulo, F. D'A. (2019). High-resolution geological investigations to reconstruct the long-term ground movements in the last 15 kyr at Campi Flegrei caldera (southern Italy). *Journal of Volcanology and Geothermal Research*. Advance online publication. https://doi.org/10.1016/j.jvolgeores.2019.07.012¶

¶

Monaco, L., Palladino, D. M., Albert, P. G., Arienzo, I., Conticelli, S., Di Vito, M., Fabbrizio, A., D'Antonio, M., Isaia, R., Manning, C. J., Nomade, S., Pereira, A., Petrosino, P., Sottili, G., Sulpizio, R., Zanchetta, G., & Giaccio, B. (2022). Linking the Mediterranean MIS 5 tephra markers to Campi Flegrei (southern Italy) 109–92 ka explosive activity and refining the chronology of MIS 5c-d millennial-scale climate variability. *Global and Planetary Change*, *211*, Article 103785. https://doi.org/10.1016/j.gloplacha.2022.103785 ¶

¶

Natale, J., Ferranti, L., Isaia, R., Marino, C., Sacchi, M., Spiess, V., Steinmann, L., & Vitale, S. (2022). Integrated on-land-offshore stratigraphy of the Campi Flegrei caldera: New insights into the volcano-tectonic evolution in the last 15 kyr. *Basin Research*, *34*(2), 855–882. https://doi.org/10.1111/bre.12643¶

¶

Natale, J., Vitale, S., Repola, L., Monti, L., and Isaia, R. (2024); Geomorphic analysis of digital elevation model generated from vintage aerial photographs: A glance at the pre-urbanization morphology of the active Campi Flegrei caldera. Geomorphology 460, 109267; https://doi.org/10.1016/j.geomorph.2024.109267 ¶

¶

Natale, J., Cascella, E., & Vitale, S. (2025); Tracking the growth and deformation of fissure phreatomagmatic eruptions: Insights from the ca. 3.9 ka Nisida eruption at Campi Flegrei caldera, southern Italy. GSA Bulletin 2025; doi: https://doi.org/10.1130/B38367.1¶

Orsi, G., Di Vito, M. A., & Isaia, R. (2004). Volcanic hazard assessment at the restless Campi Flegrei caldera. Bulletin of Volcanology, 66, 514–530. https://doi.org/10.1007/s00445-003-0327-4

Osservatorio Vesuviano (2025), Bollettino di Sorveglianza CAMPI FLEGREI GIUGNO 2025 A cura della Sezione di Napoli, available at https://www.ov.ingv.it/index.php/monitoraggio-e-infrastrutture/bollettini-tutti/bollett-mensili-cf/anno-2025-3/1850-bollettino-mensile-campi-flegrei-2025-06/file __

Pappalardo, L., Civetta, L., D'Antonio, M., Deino, A. L., Di Vito, M. A., Orsi, G., Caradente, A., De Vita, S., Isaia, R., & Piochi, M. (1999). Chemical and Sr-isotopical evolution of the Phlegraean magmatic system before the Campanian Ignimbrite (37 ka) and the Neapolitan Yellow Tuff (12 ka) eruptions. *Journal of Volcanology and Geothermal Research*, *91*(1), 141–166.¶

Rivalta, E., Corbi, F., Passarelli, L., Acocella, V., Davis, T., & Di Vito, M. A. (2019). Stress inversions to forecast magma pathways and eruptive vent location. Science Advances, 5, eaau9784. https://doi.org/10.1126/sciadv.aau9784

~~Sbrana~~Scarpati, C., Perrotta, A., ~~Marianelli~~Lepore, ~~P~~S., & ~~Pasquini~~Calvert, ~~G~~A. (~~2021~~2013). ~~The Phlegrean Fields volcanological evolution. Journal~~Eruptive history of ~~Maps~~Neapolitan volcanoes: Constraints from $^{40}Ar/^{39}Ar$ dating. *Geological Magazine*, ~~17~~*150*(~~2~~3), ~~557~~412–~~570~~425. https://doi.org/10.~~1080~~1017/~~17445647.2021.1982033~~ S0016756812000731

Selva, J., Orsi, G., Di Vito, M. A., Marzocchi, W., & Sandri, L. (2012). Probability hazard map for future vent opening at the Campi Flegrei caldera, Italy. Bulletin of Volcanology, 74, 497–510. https://doi.org/10.1007/s00445-011-0528-2

Smith, V. C., Isaia, R., & Pearce, N. J. G. (2011). Tephrostratigraphy and glass compositions of post–15 kyr Campi Flegrei eruptions: Implications for eruption history and chronostratigraphic markers. Quaternary Science Reviews, 30, 3638–3660. https://doi.org/10.1016/j.quascirev.2011.08.017 __

¶

Sparice, D., Pelullo, C., de Vita, S., Arienzo, I., Petrosino, P., Mormone, A., Di Vincenzo, G., Marfè, B., Cariddi, B., De Lucia, M., Vertechi, E., D'Oriano, C., Del Carlo, P., Di Roberto, A., Giaccio, B., Zanchetta, G., & Di Vito, M. A. (2024). The pre-Campi Flegrei caldera (>40 ka) explosive volcanic record in the Neapolitan Volcanic Area: New insights from a scientific drilling north of Naples. *Journal of Volcanology and Geothermal Research*. https://doi.org/10.1016/j.jvolgeores.2024.108209¶

Tarquini, S., Isola, I., Favalli, M., Battistini, A., & Dotta, G. (2023). TINITALY, a digital elevation model of Italy with a 10 m cell size (Version 1.1) [Data set]. Istituto Nazionale di Geofisica e Vulcanologia (INGV). https://doi.org/10.13127/tinitaly/1.1

~~Tizzani, P., Fernández, J.,~~ Vitale~~, A., Escayo, J.~~, ~~Barone, A., Castaldo, R., Pepe,~~ S., ~~De Novellis~~& Natale, ~~V., Solaro, G., Pepe, A., Tramelli, A., Hu, Z., Samsonov, S.V., Vigo, I., Tiampo, K.F., Camacho, A.GJ~~. (~~2024~~2023). ~~4D imaging of the~~Combined volcano ~~feeding system beneath~~-tectonic processes for the ~~urban area~~drowning of the Roman western coastal settlements at Campi Flegrei ~~caldera~~(southern Italy). *Earth*, ~~Remote Sensing of Environment~~*Planets and Space*, ~~315~~75, ~~114480,~~38. https://doi.org/10.~~1016~~1186/~~j.rse.2024.114480~~s40623-023-01795-7